HHS Public Access

Author manuscript

Nat Cell Biol. Author manuscript; available in PMC 2016 February 01.

Published in final edited form as:

Nat Cell Biol. 2015 August ; 17(8): 994–1003. doi:10.1038/ncb3205.

Generation of vascular endothelial and smooth muscle cells from human pluripotent stem cells

Christoph Patsch[1,6,*], **Ludivine Challet-Meylan**[2,6], **Eva C. Thoma**[1,6], **Eduard Urich**[1,6], **Tobias Heckel**[1], **John F O'Sullivan**[3], **Stephanie J Grainger**[4], **Friedrich G. Kapp**[5], **Lin Sun**[3], **Klaus Christensen**[1], **Yulei Xia**[2], **Mary H. C. Florido**[2], **Wei He**[1], **Wei Pan**[1], **Michael Prummer**[1], **Curtis R. Warren**[2], **Roland Jakob-Roetne**[1], **Ulrich Certa**[1], **Ravi Jagasia**[1], **Per-Ola Freskgård**[1], **Isaac Adatto**[3], **Dorothee Kling**[1], **Paul Huang**[3], **Leonard I Zon**[2,5], **Elliot L. Chaikof**[4], **Robert E. Gerszten**[3], **Martin Graf**[1], **Roberto Iacone**[1,6], and **Chad A. Cowan**[2,3,5,6,*]

[1]Roche Pharmaceutical Research and Early Development, Roche Innovation Center Basel, 4070 Basel, Switzerland [2]Department of Stem Cell and Regenerative Biology and Harvard Stem Cell Institute, Harvard University, Massachusetts 02138, USA [3]Cardiovascular Research Center and Cardiology Division, Massachusetts General Hospital and Harvard Medical School, Boston, USA [4]Department of Surgery, Beth Israel Deaconess Medical Center, Harvard Medical School, 110 Francis St, Suite 9F, Boston, MA 02115 (USA); the Wyss Institute of Biologically Inspired Engineering of Harvard University, Boston, MA (USA) [5]Stem Cell Program and Division of Hematology/Oncology, Boston Children's Hospital and Dana Farber Cancer Institute, Howard Hughes Medical Institute, Harvard Medical School, Boston, MA 02115, USA

Abstract

The use of human pluripotent stem cells for *in vitro* disease modeling and clinical applications requires protocols that convert these cells into relevant adult cell types. Here, we report the rapid and efficient differentiation of human pluripotent stem cells into vascular endothelial and smooth muscle cells. We found that GSK3 inhibition and BMP4 treatment rapidly committed pluripotent cells to a mesodermal fate and subsequent exposure to VEGF or PDGF-BB resulted in the differentiation of either endothelial or vascular smooth muscle cells, respectively. Both protocols produced mature cells with efficiencies over 80% within six days. Upon purification to 99% via

[*]Correspondence: christoph.patsch@roche.com or chad_cowan@harvard.edu.
[6]These authors contributed equally to this work

Author Contributions

C.P., L.C-M., E.C.T., and E.U. designed and performed experiments, analyzed and interpreted data and wrote the manuscript. S.J.G., F.G.K., L.S., K.C., Y.X., M.H.C.F., W.H., W.P., C.R.W., R.J-R., and I.A. designed and performed experiments and analyzed data. M.P. performed high-content imaging analysis. T.H: designed and performed gene expression experiments, performed and interpreted bioinformatic analyses and wrote the manuscript. J.F.O. designed and performed metabolomic experiments, interpreted and analyzed the data and wrote the manuscript. U.C. and R.J. provided scientific input. P.O.F., D.K., P.H., L.I.Z., E.L.C. and R.E.G. analyzed and interpreted the data and supervised experiments. M.G. and R.I. analyzed and interpreted the data and supervised the project. C.A.C. interpreted the data, supervised the project and wrote the manuscript. C.P., L.C-M., E.C.T, E.U., J.F.O., M.P., D.K., T.H. and W.H. contributed to description of online methods.

Competing Financial Interests

The other authors report no relevant conflicts of interest.

surface markers, endothelial cells maintained their identity, as assessed by marker gene expression, and showed relevant *in vitro* and *in vivo* functionality. Global transcriptional and metabolomic analyses confirmed that the cells closely resembled their *in vivo* counterparts. Our results suggest that these cells could be used to faithfully model human disease.

Introduction

Human pluripotent stem cells (hPSCs)[12,3] have unlimited proliferation capacity and the potential to differentiate into all somatic cell types. Ideally, they can be used to generate an inexhaustible supply of cells for clinical and scientific applications. Patient–specific hPSCs promise to reveal the molecular and genetic basis of disease. However, a prerequisite for exploiting their potential to understand disease is the development of strategies for directing their differentiation into functional adult cell types [4–6]. In addition to being reproducible, simple and quick, ideal differentiation strategies would yield pure populations of cells in sufficient quantities to enable high-throughput screening and large-scale analyses. Thus, a major obstacle for using hPSCs to model disease remains the lack of reliable, efficient and scalable protocols to differentiate functionally mature adult cell types.

Blood vessels deliver oxygen and nutrients to all of the tissues and organs in the body. The two major cellular components of blood vessels are endothelial cells (ECs) and vascular smooth muscle cells (VSMCs). Both ECs and VSMCs are required for vascular function, including blood pressure control, interactions with immune cells, and the uptake of nutrients. Consequently, these cells are involved in a variety of pathological dysfunctions, including the most common cardiovascular disease, atherosclerosis. To date, there exist two commonly used methods to induce vascular cell differentiation from hPSCs: 1) embryoid body (EB) formation [7,8] and 2) monolayer-directed differentiation [9,10]. EB formation results in differentiation of hPSCs into various cell types, including vascular cells, albeit inefficiently (1%–5%) [7,11,12]. Moreover, EB differentiation is often time-consuming, with peak expression of endothelial genes occurring after 10–15 days [13]. Current monolayer differentiation methods offer increased efficiencies (5–20%) but depend on undefined supplements, co-culture [10,14,15], heterogeneous cell aggregates [16], conditioned medium [9,17], or lack consistent yields of vascular cells [18]. Thus, improved methods would increase differentiation fidelity, efficiency and kinetics.

In mammalian development, vascular progenitors emerge from the lateral and posterior mesoderm [19]. Several studies describe the importance of canonical Wnt signaling in mesoderm commitment during embryogenesis [20]. For example, mice with impaired Wnt signaling lack mesoderm [21,22]. Canonical Wnt signaling in hPSCs induces mesendoderm [23], cardiogenesis [24] and the formation of vascular cells[16]. Based on previous reports[25, 26,27] we sought to develop a protocol for the differentiation of hPSCs to vascular cells. Here, we describe the rapid and efficient conversion of hPSCs into vascular cells using chemically defined conditions. Our protocol utilizes GSK3 inhibition and BMP4 treatment to convert hPSCs into mesodermal cells that when exposed to VEGF or PDGF-BB produced functional ECs or VSMCs.

Results

Canonical Wnt activation and mesoderm induction by pharmacological inhibition of GSK3

Wnt signaling directs differentiation of hPSCs into mesoderm and GSK3ß inhibition activates this pathway [16,23]. However, small molecule inhibitors of GSK3 can either promote self-renewal or mesendodermal differentiation of hPSCs [16,28,29]. We therefore attempted to identify selective GSK3ß inhibitors that promoted efficient commitment of hPSCs towards mesoderm. A panel of GSK3 inhibitors was evaluated for their selectivity and potential to inhibit GSK3 and to activate Wnt signaling (Supplementary Table 1).

An *in vitro* competition binding assay against 96 protein kinases was performed to evaluate the specificity of GSK3 inhibitors, including 6-bromoindirubin-3′-oxime (BIO), CHIR-99021 (CHIR) [30], SB216763 [31] and a Roche compound, CP21R7 (CP21) (Supplementary Figure 1A). CP21 and CHIR were the most selective GSK3 inhibitors (Supplementary Table 2). CP21 also showed the highest affinity to GSK3ß followed by the CHIR (Supplementary Figure 1D). These findings indicate that CP21 and CHIR are high-affinity, selective GSK3ß inhibitors.

To examine these compounds capacity to activate canonical Wnt signaling, a dose-response assay was performed using a reporter cell line [32] with the luciferase gene expressed by a TCF/LEF promoter (Supplementary Figure 1B). Compound CP21, BIO and CHIR were able to potently activate canonical Wnt signaling with highest activity at 3μM (CP21, BIO) and 10μM (CHIR). In contrast, the compounds SB, AR-AO14418 and MeBIO did not induce TCF/LEF luciferase expression (Figure 1A). The increase in TCF/LEF::luciferase activation by GSK3 inhibitors was not due to global transcriptional activation as measured in Gli-luciferase responsive reporter cells (Supplementary Figure 1C). Furthermore, the compounds did not affect cell viability except BIO, which was toxic at concentrations above 3 μM (Supplementary Figures 1C and 1E). Thus, CP21, CHIR and BIO were able to activate canonical WNT signaling to similar levels, but given the toxicity of BIO we chose not to include this compound in subsequent experiments. Next, we analyzed protein levels of ß-catenin in hPSCs treated with CP21 and CHIR. Immunofluorescence staining revealed that CP21 and CHIR significantly increased total levels of intracellular ß-catenin (Figure 1B). This result was confirmed by gene expression analyses (Figure 1C), wherein Wnt target genes were upregulated following CP21 and CHIR treatment of hPSCs. Thus, CP21 and CHIR potently and selectively inhibit GSK3 to activate canonical Wnt signaling.

We next investigated whether GSK3 inhibition with CP21 and CHIR in hPSCs would induce mesoderm. As BMP4 is also a potent inducer of mesoderm [33], we tested BMP4 alone or combined with WNT activation by CP21 and CHIR. Gene expression analyses revealed that BMP4 treatment with WNT activation led to upregulation of genes associated with mesoderm, such as *T, MIXL*, and *EOMES* (Supplementary Figure 2A). Immunostaining of CP21 and BMP4 treated cells showed high levels of BRACHYURY (T) expression which peaked at day three (Figure 1D). Conversely, OCT4 was downregulated. SOX17 was not detected indicating that the cells were likely mesodermal (Figure 1D). Similar results were obtained using CHIR and BMP4 (Figure 1D). Thus, activation of WNT signaling via GSK3

inhibition with CP21 or CHIR combined with BMP4 induced commitment of hPSCs towards mesoderm.

Efficient differentiation of mesodermal progenitors to endothelial cells or vascular smooth muscle cells

We assessed the ability of hPSC-derived mesoderm to undergo vascular lineage commitment using a chemically defined protocol consisting of three steps. First, hPSCs were plated as single cells at a density of 37,000 cells per cm^2 with Rho-kinase inhibitor Y-27632 [34], second, cells were differentiated to mesoderm using either CP21 or CHIR and/or BMP4, and third, they were treated with VEGF to induce ECs [16]. At day five, EC differentiation was evaluated by analyzing the expression of vascular endothelial-cadherin (VE-Cadherin, CD144). $CD144^+$ cells were readily detected in CHIR and CP21 treated cultures, but were absent in controls (Supplementary Figure 2B). Flow cytometric analysis of CD144 expression revealed that only BMP4 and CP21 or CHIR combined were capable of inducing high levels of expression, whereas treatment with BMP4 alone led to fewer than 10% $CD144^+$ cells (Supplementary Figure 2C). Additional analysis identified CP21 as the most potent compound (Supplementary Figure 2D) with a concentration of 1μM yielding up to 35% $CD144^+$ cells, whereas CHIR induced CD144 expression most efficiently at a concentration of 6μM. When either GSK3 inhibitor was used at its optimal concentration the yield of $CD144^+$ cells was equivalent (Supplementary Figure 2E).

We next combined VEGF treatment with Forskolin for two days, as protein kinase A activation via cyclic AMP leads to an increase in vascular development [35], followed by VEGF treatment alone for an additional four days (Supplementary Figure 2F). We tested this strategy on several hPSC lines, including HUES9, SA001, BJ-RiPS, and a commercially available iPS cell line [3637]. This protocol promoted the differentiation of hPSCs into endothelial cells with efficiencies between 61.8% and 88.8% (SEM 3.1, n=10 independent experiments) as assessed by flow cytometry of CD144+ cells (Figure 2A, B and Supplementary Table 4A). CD144+ cells were further analyzed for expression of EC specific markers. Flow cytometry revealed hPSC-derived ECs expressed KDR, CD31, CD34, and CD105. Expression of the hematopoietic lineage markers CD43 and CD45 was not detected (Supplementary Figure 2G). Immunostaining revealed that the cells were also positive for EC markers vWF and PECAM1 (Figure 2C). Overall, these results demonstrate that GSK3 inhibition and BMP4 treatment followed by a brief period VEGF and Forskolin exposure and continued VEGF treatment is sufficient to rapidly and efficiently induce ECs from hPSCs (Figure 2E).

Interestingly, immunostaining revealed that in addition to ECs a small fraction of cells expressed the vascular smooth muscle marker smooth muscle-actin (SMA) (Supplementary Figure 2H). We reasoned that replacing endothelial inductive cues with factors that promote VSMC formation we might efficiently generate VSMCs. ActivinA and PDGF-BB have been shown to promote the formation of VSMCs [383940]. Thus, we added ActivinA and/or PDGF-BB following mesoderm induction. Strikingly, this modification resulted in the formation of almost exclusively CD140b+ (PDGFRB) cells with virtually no $CD144^+$ cells detectable when ActivinA and PDGF-BB were used (Figure 2A, B and Supplementary Figure 2I and

2J). The differentiation of CD140b+ cells required either CP21 or CHIR and was not induced following treatment with BMP4 alone (Supplementary Figure 2K). The cells also expressed other markers of VSMCs, such as SMA and Myosin IIB (Figure 2D). The efficiency of differentiation of VSMCs was similar across hPSC lines, with on average 95.4% CD140b+ cells generated (SEM 2.7, n=16 independent experiments) (Supplementary Table 4B). Thus, GSK3 inhibition and BMP4 treatment followed by ActivinA and PDGF-BB treatment rapidly and efficiently induced VSMCs from hPSCs (Figure 2F).

To purify hPSC-derived ECs, we performed magnetic associated cell sorting (MACS) at day six of differentiation. After MACS-mediated selection for CD144 expressing cells, we obtained virtually pure (on average 95.9%, SEM 3.0, n=19 independent experiments) EC cultures (Supplementary Figure 2L and Supplementary Table 4C). As hPSC-VSMCs cultures were nearly homogeneous they required no further purification.

A step-by-step protocol describing the culture of hESCs and the differentiation of hPSC-ECs (doi:10.1038/protex.2015.055) and hPSC-VSMCs (doi:10.1038/protex.2015.056) can be found at Nature Protocol Exchange.

hPSCs-derived ECs and VSMCs display a transcriptional signature similar to primary vascular cells

To evaluate hPSC-derived vascular cells and monitor differentiation dynamics on a molecular level, we performed gene expression profiling at seven time points during differentiation. A projection of the complete expression profiles onto the first two principal components following principle component analysis revealed that differentiating cells cluster until day 4 with hPSCs. However, upon induction into ECs or VSMCs, the cells became highly similar to their corresponding primary cells as shown by principal component projections after two weeks of differentiation (Supplementary Figure 3A). This similarity is also reflected by the Pearson correlation coefficient for all expressed genes between primary and hPSC-derived ECs (r = 0.93) or primary and hPSC-derived VSMCs (r = 0.88). Of note, cultured primary cells do not perfectly mimic their *in vivo* counterparts.

To examine mesoderm commitment a time-course of gene expression was plotted for representative genes from pluripotent cells, mesoderm, neuroectoderm, endoderm, endothelium and regionalization of the primitive streak (Supplementary Figure 3B). These analyses revealed that pluripotent cell markers such as *NANOG*, *UTF1* and *SOX2* were rapidly down-regulated. *OCT4* expression was less rapidly down-regulated and decreased by day 10. We observed a transient activation of the genes found in mesoderm, such as *MIXL1*, *T/BRACHYURY*, *FGF4* and *EOMES*. With the exception of the endodermal marker *SOX17*, which was highly expressed at day five of EC differentiation, expression of markers associated with neuroectoderm or endoderm was not observed. Expression of *SOX17* mimics the *in vivo* pattern found in the developing and adult vasculature [41]. We did not observe differentiation of trophectoderm or visceral endoderm, as *ESX1* and *SOX7* were undetectable. These data support the differentiation of hPSCs via a mesodermal intermediate into ECs or VSMCs.

We found that 2955 genes were differentially expressed by at least 10-fold between hPSCs, differentiated ECs, VSMCs and primary cells (Figure 3A). These genes were hierarchically clustered and analyzed on the basis of Gene Ontology (GO) terms using the DAVID Bioinformatics Resource. The most prominently enriched gene sets included annotations for blood vessel development (GO:0001568, $p < 10^{-19}$) and cell adhesion (GO:0007155, $p < 10^{-10}$) for ECs, extracellular matrix organization (GO:0030198, $p < 10^{-11}$) and muscle organ development (GO:0007517; $p < 10^{-8}$) for VSMCs, and cell projection organization (GO:0030030; $p < 10^{-9}$), cell adhesion (GO:0007155, $p < 10^{-13}$) and the cell cycle process (GO:0007049; $p < 10^{-6}$) for hPSCs (Figure 3B).

We performed gene set enrichment analysis to find genes defined by biological processes within those genes that were either up- or down-regulated Only gene-sets passing significance thresholds with a p-value of 0.001 and a false discovery rate of 0.05 were selected as biological processes significantly over- or under-represented in hPSC-derived ECs, VSMCs, and primary cells versus hPSCs. Positively enriched gene sets for hPSC-derived and primary ECs included endothelial cell differentiation (GO:0045446), angiogenesis (GO:0001525), endothelium development (GO:0003158) and blood vessel development (GO:0001568). For all VSMCs, top enriched gene sets were extracellular matrix (GO:0030198), collagen fibril organization (GO:0030199), regulation of smooth muscle cell migration (GO:0014911) and proliferation (GO:0048660). Most significantly down-regulated gene-sets in hPSC- derived ECs and VSCMs were gene sets for mitosis (GO:0007067) and chromosome segregation (GO:0007059) (Supplementary Table 3 and Supplementary Figure 3C).

In summary, transcriptome-wide expression analysis demonstrated that hPSC-derived ECs and VSMCs were highly similar to their respective primary cells.

hPSC-derived ECs and VSMCs diplay a metabolomic profile similar to primary vascular cells

We performed metabolomic analysis via liquid chromatography-tandem mass spectrometry (LC-MS) of hPSC-derived vascular and primary cells. Of 106 metabolites, we detected 66 intracellularly (Supplementary Table 5). There was a strong correlation between metabolite levels in primary ECs and in hPSC-derived ECs (Spearman coefficient HUVEC v hPSC-EC = 0.96, HCAEC v hPSC-EC = 0.98, Figure 3C and D), and also between metabolite concentrations in primary VSMCs (UASMCs) and in hPSC-VSMCs (Spearman coefficient = 0.92, Figure 3C and D). These similarities were seen across metabolite classes, including amino acids, amino acid derivatives, nucleosides, organic nitrogenous compounds, aromatic acids, amine oxides, and other organic acids (Supplementary Table 5). In contrast, hPSCs had a distinct metabolic profile when compared to hPSC-ECs (Spearman coefficient = 0.80) or hPSC-VSMCs (Spearman coefficient AUSMC (contractile) v hPSC-VSMC (contractile) = 0.97, AUSMC (synthetic) v hPSC-VSMC (synthetic) = 0.97, Figure 3C and D). Thus, these analyses indicate that hPSC-derived vascular cells have metabolic profiles that closely resemble primary ECs and VSMCs.

hPSC-derived ECs and VSMCs exhibit mature functional properties

We sought to analyze the functional capabilities of hPSC-derived vascular cells. To determine barrier function of hPSC-ECs we measured impedance using an xCeLLigence RT-CA system [42,43]. The formation of a tight monolayer was observed by an increase in impedance within four hours after plating. Monolayer impedance reached a plateau, which was maintained for several days without major fluctuations (Figure 4A). Treatment with the vasoactive agent thrombin led to a rapid and reversible decrease in impedance [44]. Analysis of trans-endothelial electrical resistance (TEER) revealed that hPSC-ECs showed TEER values similar to primary ECs (HUVECs). Treatment with cytokines TNF-α, VEGF-A, and IL1ß led to disruption of barrier tightness as revealed by decrease in TEER values (Figure 4B). We then analyzed further *in vitro* functional features of hPSC-ECs. The capacity of lipid uptake was monitored using fluorescently labeled acetylated LDL (Figure 4C).

To determine whether hPSC-ECs respond to proinflammatory cytokines with a pro-adhesive phenotype, we challenged the hPSC-ECs with TNF-α and IL-1ß. Immunofluorescence analysis showed an increased expression of intracellular adhesion molecule-1 (ICAM1) upon TNF-α treatment (Figure 4D). Flow cytometric analysis results confirmed the upregulation of ICAM1 upon TNF-α and IL-1ß stimulation (Figure 4E). We co-cultured hPSC-ECs with leukocyte-like HL60 cells to examine cellular adhesion molecule-mediated tethering and capture[45, 46]. Remarkably, adhesion of HL60 cells was significantly enhanced when hPSC-derived ECs were stimulated with TNF-α (Figure 4F). Application of ICAM1-specific antibodies reduced adhesion of HL60 cells in a concentration-dependent manner suggesting that leukocyte adhesion was indeed mediated by ICAM1 (Figure 4G).

Next, we analyzed contractility of hPSC-VSMCs by stimulation with vasoconstrictive drugs or cytokines (Figure 4H and Supplementary Figure 4A). Calcium imaging revealed that Endothelin1 and carbachol induced an increase in intracellular calcium levels. Treatment with atropin prevented carbachol mediated calcium influx. Utilizing a 3-dimensional collagen contractility assay, hPSC-VSMCs contracted similarly to primary VSMCs when exposed to a vasoconstrictor (U46619; Figure 4I and Supplementary Figure 4B). Thus, hPSC-derived VSMCs are capable of responding to vasoconstrictive stimuli displaying a key functional *in vivo* characteristic.

Deposition of extracellular fibronectin (FN) was analysed following treatment of hPSC-VSMCs with increasing concentrations of TGF-ß (Supplementary Figure 4C). Interestingly, FN depositions could be detected even in untreated cultures. As VSMCs produce TGF-ß this is likely due to autocrine TGF-ß signaling [47]. Treatment with exogenous TGF-ß led to a slight increase in FN production. Addition of small molecules inhibiting TGF-ß signaling (SB525334 or JQ1) prevented FN production in the presence and absence of exogenous TGF-ß. Thus, FN deposition of hPSC-VSMCs is mediated by TGF-ß.

In summary, these findings show that hPSC-derived ECs and VSMCs demonstrate key mature functional properties.

hPSC-ECs form vascular structures *in vitro* and *in vivo* after transplantation

Tube formation assays were performed to determine the angiogenic potential of hPSC-ECs. Formation of vascular network-like structures was observed within 24hours and could be perturbed by treatment with sulforaphane and an anti-VEGF monoclonal antibody (Figure 5A and B). Remarkably, when hPSC-ECs were co-cultured with primary human brain vascular pericytes (hBVPs) both cell types arranged in highly organized structures with hBVPs tightly associated to endothelial tubes (Figure 5C). HBVPs cells appeared to envelope hPSC-EC tubes (Figure 5D). These results demonstrate that hPSC-ECs have angiogenic potential *in vitro*. To evaluate this potential *in vivo*, we utilized fibrinogen grafts in immunodeficient NOD-SCID mice[48]. We implanted either hPSC-ECs alone, HUVECs and MSCs, hPSC-ECs and MSCs, or hPSC-ECs and hPSC-VSMCs into dorsal side of NOD-SCID mice and recovered the grafts for analysis after 14 days (except for hPSC-ECs alone = 7 days) (Supplementary Figure 5)[48]. Hematoxylin and eosin staining showed vessel-like networks in implants containing HUVECs and MSCs, hPSC-ECs and MSCs, and hPSC-ECs and hPSC-VSMCs (Figure 5G, I, and K). Of note, vessels contained numerous circulating red blood cells. Staining with an antibody for human CD31 revealed vessel-like structures throughout the implants (Figure 5H, J and L). Thus, hPSC-ECs are capable of contributing to patent, blood containing vessel-like networks *in vivo*.

Discussion

We report the rapid and efficient differentiation of hPSCs to ECs and VSMCs. GSK3β inhibition combined with BMP4 treatment enabled the commitment of hPSCs to mesoderm. Subsequently, differentiation was directed by treatment with VEGF for ECs or PDGF-BB and ActivinA for VSMCs. This *in vitro* differentiation pathway showed similarities to vascular development *in vivo*. For instance, Wnt signaling is required to induce primitive streak formation [20], which then becomes committed lateral plate mesoderm via BMP4 signaling these events were also observed during our *in vitro* differentiation protocol. Genome-wide expression analysis revealed transiently expressed gene clusters linked to mesoderm formation and further regionalization into lateral plate mesoderm. Subsequently, EC and VSMC formation was indicated by increased expression of genes associated with vasculogenesis. Importantly, our protocol produced ECs and VSMCs that closely resembled their primary counterparts. Comprehensive functional characterization of hPSC-derived vascular cells indicated a *bona fide* vascular phenotype. Taken together, these experiments confirm the identity and maturity of the hPSC-derived ECs and VSMCs and suggest that the cells could be used to faithfully model human disease.

Compared to other protocols that induce vascular cells from hPSCs, our approach provides several advantages. First, it occurs under chemically defined conditions in monolayer culture with low variability. While a recently published report utilizes chemically defined conditions and starts with a monolayer culture, they observed considerable variation between experiments and starting cell lines and only achieved efficiencies of 10–30%[18]. Second, our protocol allows the formation of ECs and VSMCs in a process closely

resembling *in vivo* development. Last, our method allows rapid vascular differentiation with high efficiency. We obtained from 1 million hPSCs approximately 25–30 million ECs or VSMCs within 6 days, cutting the time to generate these cells in half as compared to published protocols[18]. As hPSC-derived ECs and VSMCs can be purified to near homogeneity by immunomagnetic cell sorting, the protocol is not only efficient but scalable. The method therefore represents a valuable tool for application of stem cells in assays such as disease modeling or high-throughput screening where the availability of large numbers of defined cell types is a key prerequisite. This approach is likely to serve as a new standard for deriving endothelial cells and vascular smooth muscle cells at scales relevant for drug discovery and regenerative therapies.

Supplementary Material

Refer to Web version on PubMed Central for supplementary material.

Acknowledgments

We thank Alfred Einhaus, Silke Zimmermann, Corinne Stücki as well as Nadine Dahm for excellent technical support and all members of the Roche Stem Cell Platform for helpful discussions. We thank Cathy MacGillivray at the HSCRB Histology Core facility. We also thank Stefan Aigner and Curtis Warren for critically reviewing the manuscript and Anna Gündner, Carolyn Hudak and Kuncheng Song for help with the illustrations. We acknowledge the continued support of Hoffmann-La Roche and thank Matthias Steger from Roche Pharma Partnering for his input and support of the project. C.P. and E.C.T were supported by Roche Postdoctoral Fellowships (RPF). A part of the research received support from the Innovative Medicines Initiative Joint Undertaking under grant agreement no °115439, resources of which are composed of financial contribution from the European Union's Seventh Framework Program (FP7/2007–2013) and EFPIA companies' in kind contribution. L.C-M was supported by a fellowship from the Swiss National Science Foundation. F.G.K. was supported by a fellowship from the German Cancer Aid. This work was supported by HHMI and NIH grants R01 HL04880, 5P30 DK49216, 5R01 DK53298, 5U01 HL10001-05, and R24 DK092760 (to L.I.Z.) and HL106018, HL083867, HL60963 (E.L.C) and 2R01DK081572 and an AHA Established Investigator Award (R.G) and R01DK097768 and U01HL100408 (C.A.C.) and the Harvard Stem Cell Institute (C.A.C.) and Harvard University (C.A.C.).

References

1. Thomson JA, et al. Embryonic stem cell lines derived from human blastocysts. Science. 1998; 282:1145–1147. [PubMed: 9804556]
2. Takahashi K, et al. Induction of pluripotent stem cells from adult human fibroblasts by defined factors. Cell. 2007; 131:861–872.10.1016/j.cell.2007.11.019 [PubMed: 18035408]
3. Yu J, et al. Induced pluripotent stem cell lines derived from human somatic cells. Science. 2007; 318:1917–1920.10.1126/science.1151526 [PubMed: 18029452]
4. Grskovic M, Javaherian A, Strulovici B, Daley GQ. Induced pluripotent stem cells–opportunities for disease modelling and drug discovery. Nature reviews Drug discovery. 2011; 10:915–929.10.1038/nrd3577 [PubMed: 22076509]
5. Tiscornia G, Vivas EL, Belmonte JC. Diseases in a dish: modeling human genetic disorders using induced pluripotent cells. Nat Med. 2011; 17:1570–1576.10.1038/nm.2504 [PubMed: 22146428]
6. Zhu H, Lensch MW, Cahan P, Daley GQ. Investigating monogenic and complex diseases with pluripotent stem cells. Nature Reviews Genetics. 2011; 12:266–275.10.1038/nrg2951
7. James D, et al. Expansion and maintenance of human embryonic stem cell-derived endothelial cells by TGFbeta inhibition is Id1 dependent. Nat Biotechnol. 2010; 28:161–166.10.1038/nbt.1605 [PubMed: 20081865]
8. Levenberg S, Golub JS, Amit M, Itskovitz-Eldor J, Langer R. Endothelial cells derived from human embryonic stem cells. Proc Natl Acad Sci U S A. 2002; 99:4391–4396.10.1073/pnas.032074999 [PubMed: 11917100]

9. Kane NM, et al. Derivation of endothelial cells from human embryonic stem cells by directed differentiation: analysis of microRNA and angiogenesis in vitro and in vivo. Arterioscler Thromb Vasc Biol. 2010; 30:1389–1397.10.1161/ATVBAHA.110.204800 [PubMed: 20431067]
10. Vodyanik MA, Bork JA, Thomson JA, Slukvin II. Human embryonic stem cell-derived CD34+ cells: efficient production in the coculture with OP9 stromal cells and analysis of lymphohematopoietic potential. Blood. 2005; 105:617–626.10.1182/blood-2004-04-1649 [PubMed: 15374881]
11. Li Z, et al. Comparison of reporter gene and iron particle labeling for tracking fate of human embryonic stem cells and differentiated endothelial cells in living subjects. Stem cells. 2008; 26:864–873.10.1634/stemcells.2007-0843 [PubMed: 18218820]
12. Wang H, et al. Gene expression profile signatures indicate a role for Wnt signaling in endothelial commitment from embryonic stem cells. Circulation research. 2006; 98:1331–1339.10.1161/01.RES.0000220650.26555.1d [PubMed: 16601226]
13. Levenberg S, Zoldan J, Basevitch Y, Langer R. Endothelial potential of human embryonic stem cells. Blood. 2007; 110:806–814.10.1182/blood-2006-08-019190 [PubMed: 17412888]
14. Kelly MA, Hirschi KK. Signaling hierarchy regulating human endothelial cell development. Arterioscler Thromb Vasc Biol. 2009; 29:718–724.10.1161/ATVBAHA.109.184200 [PubMed: 19213939]
15. Wang ZZ, et al. Endothelial cells derived from human embryonic stem cells form durable blood vessels in vivo. Nat Biotechnol. 2007; 25:317–318.10.1038/nbt1287 [PubMed: 17322871]
16. Sumi T, Tsuneyoshi N, Nakatsuji N, Suemori H. Defining early lineage specification of human embryonic stem cells by the orchestrated balance of canonical Wnt/beta-catenin, Activin/Nodal and BMP signaling. Development. 2008; 135:2969–2979.10.1242/dev.021121 [PubMed: 18667462]
17. <2002_Inman_SB-431542 is a potent and specific inhibitor of transforming growth factor-beta superfamily type I activin receptor-like kinase (ALK) receptors ALK4, ALK5, and ALK7-pdf.pdf>.
18. Orlova VV, et al. Functionality of endothelial cells and pericytes from human pluripotent stem cells demonstrated in cultured vascular plexus and zebrafish xenografts. Arterioscler Thromb Vasc Biol. 2014; 34:177–186.10.1161/ATVBAHA.113.302598 [PubMed: 24158517]
19. Yamashita J, et al. Flk1-positive cells derived from embryonic stem cells serve as vascular progenitors. Nature. 2000; 408:92–96.10.1038/35040568 [PubMed: 11081514]
20. Tam PP, Loebel DA. Gene function in mouse embryogenesis: get set for gastrulation. Nature reviews Genetics. 2007; 8:368–381.10.1038/nrg2084
21. Huelsken J, et al. Requirement for beta-catenin in anterior-posterior axis formation in mice. The Journal of cell biology. 2000; 148:567–578. [PubMed: 10662781]
22. Liu Y, Festing MH, Hester M, Thompson JC, Weinstein M. Generation of novel conditional and hypomorphic alleles of the Smad2 gene. Genesis. 2004; 40:118–123.10.1002/gene.20072 [PubMed: 15452874]
23. Woll PS, et al. Wnt signaling promotes hematoendothelial cell development from human embryonic stem cells. Blood. 2008; 111:122–131.10.1182/blood-2007-04-084186 [PubMed: 17875805]
24. Brade T, Manner J, Kuhl M. The role of Wnt signalling in cardiac development and tissue remodelling in the mature heart. Cardiovasc Res. 2006; 72:198–209.10.1016/j.cardiores.2006.06.025 [PubMed: 16860783]
25. Park C, et al. A hierarchical order of factors in the generation of FLK1- and SCL-expressing hematopoietic and endothelial progenitors from embryonic stem cells. Development. 2004; 131:2749–2762.10.1242/dev.01130 [PubMed: 15148304]
26. Tada S, et al. Characterization of mesendoderm: a diverging point of the definitive endoderm and mesoderm in embryonic stem cell differentiation culture. Development. 2005; 132:4363–4374.10.1242/dev.02005 [PubMed: 16141227]
27. Nostro MC, Cheng X, Keller GM, Gadue P. Wnt, activin, and BMP signaling regulate distinct stages in the developmental pathway from embryonic stem cells to blood. Cell Stem Cell. 2008; 2:60–71.10.1016/j.stem.2007.10.011 [PubMed: 18371422]

28. Bone HK, Nelson AS, Goldring CE, Tosh D, Welham MJ. A novel chemically directed route for the generation of definitive endoderm from human embryonic stem cells based on inhibition of GSK-3. Journal of cell science. 2011; 124:1992–2000.10.1242/jcs.081679 [PubMed: 21610099]
29. Sato N, Meijer L, Skaltsounis L, Greengard P, Brivanlou AH. Maintenance of pluripotency in human and mouse embryonic stem cells through activation of Wnt signaling by a pharmacological GSK-3-specific inhibitor. Nat Med. 2004; 10:55–63.10.1038/nm979 [PubMed: 14702635]
30. Fabian MA, et al. A small molecule-kinase interaction map for clinical kinase inhibitors. Nat Biotechnol. 2005; 23:329–336.10.1038/nbt1068 [PubMed: 15711537]
31. Soker S, Takashima S, Miao HQ, Neufeld G, Klagsbrun M. Neuropilin-1 is expressed by endothelial and tumor cells as an isoform-specific receptor for vascular endothelial growth factor. Cell. 1998; 92:735–745. [PubMed: 9529250]
32. DeAlmeida VI, et al. The soluble wnt receptor Frizzled8CRD-hFc inhibits the growth of teratocarcinomas in vivo. Cancer research. 2007; 67:5371–5379.10.1158/0008-5472.CAN-07-0266 [PubMed: 17545618]
33. Winnier G, Blessing M, Labosky PA, Hogan BL. Bone morphogenetic protein-4 is required for mesoderm formation and patterning in the mouse. Genes & development. 1995; 9:2105–2116. [PubMed: 7657163]
34. Watanabe K, et al. A ROCK inhibitor permits survival of dissociated human embryonic stem cells. Nat Biotechnol. 2007; 25:681–686.10.1038/nbt1310 [PubMed: 17529971]
35. Yamamizu K, Kawasaki K, Katayama S, Watabe T, Yamashita JK. Enhancement of vascular progenitor potential by protein kinase A through dual induction of Flk-1 and Neuropilin-1. Blood. 2009; 114:3707–3716.10.1182/blood-2008-12-195750 [PubMed: 19706882]
36. Englund MC, et al. The establishment of 20 different human embryonic stem cell lines and subclones; a report on derivation, culture, characterisation and banking. In vitro cellular & developmental biology Animal. 2010; 46:217–230.10.1007/s11626-010-9289-z [PubMed: 20177996]
37. Burridge PW, et al. A universal system for highly efficient cardiac differentiation of human induced pluripotent stem cells that eliminates interline variability. PLoS One. 2011; 6:e18293.10.1371/journal.pone.0018293 [PubMed: 21494607]
38. Chan MC, et al. Molecular basis for antagonism between PDGF and the TGFbeta family of signalling pathways by control of miR-24 expression. Embo J. 2010; 29:559–573.10.1038/emboj.2009.370 [PubMed: 20019669]
39. Owens GK, Kumar MS, Wamhoff BR. Molecular regulation of vascular smooth muscle cell differentiation in development and disease. Physiol Rev. 2004; 84:767–801.10.1152/physrev.00041.2003 [PubMed: 15269336]
40. Cheung C, Bernardo AS, Trotter MW, Pedersen RA, Sinha S. Generation of human vascular smooth muscle subtypes provides insight into embryological origin-dependent disease susceptibility. Nat Biotechnol. 2012; 30:165–173.10.1038/nbt.2107 [PubMed: 22252507]
41. Engert S, Liao WP, Burtscher I, Lickert H. Sox17-2A-iCre: a knock-in mouse line expressing Cre recombinase in endoderm and vascular endothelial cells. Genesis. 2009; 47:603–610.10.1002/dvg.20540 [PubMed: 19548312]
42. Atienza JM, et al. Dynamic and label-free cell-based assays using the real-time cell electronic sensing system. Assay and drug development technologies. 2006; 4:597–607.10.1089/adt.2006.4.597 [PubMed: 17115930]
43. Solly K, Wang X, Xu X, Strulovici B, Zheng W. Application of real-time cell electronic sensing (RT-CES) technology to cell-based assays. Assay and drug development technologies. 2004; 2:363–372.10.1089/1540658041850544 [PubMed: 15357917]
44. Rabiet MJ, et al. Thrombin-induced increase in endothelial permeability is associated with changes in cell-to-cell junction organization. Arterioscler Thromb Vasc Biol. 1996; 16:488–496. [PubMed: 8630677]
45. Galkina E, Ley K. Vascular adhesion molecules in atherosclerosis. Arterioscler Thromb Vasc Biol. 2007; 27:2292–2301.10.1161/ATVBAHA.107.149179 [PubMed: 17673705]
46. Lusis AJ. Atherosclerosis. Nature. 2000; 407:233–241.10.1038/35025203 [PubMed: 11001066]

47. Rasmussen LM, Wolf YG, Ruoslahti E. Vascular smooth muscle cells from injured rat aortas display elevated matrix production associated with transforming growth factor-beta activity. The American journal of pathology. 1995; 147:1041–1048. [PubMed: 7573349]

48. Grainger SJ, Carrion B, Ceccarelli J, Putnam AJ. Stromal cell identity influences the in vivo functionality of engineered capillary networks formed by co-delivery of endothelial cells and stromal cells. Tissue Eng Part A. 2013; 19:1209–1222.10.1089/ten.TEA.2012.0281 [PubMed: 23216113]

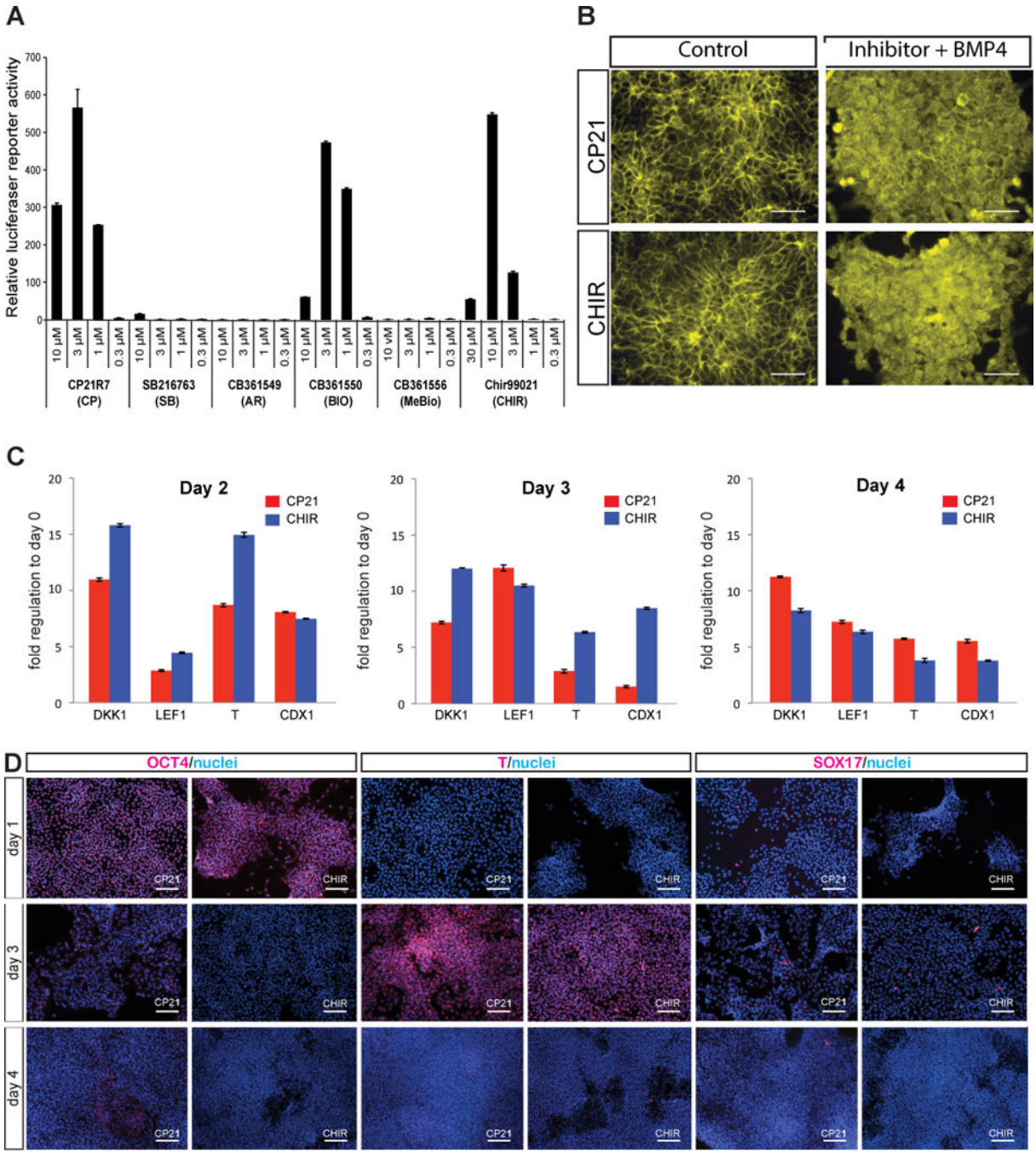

Figure 1. Canonical Wnt activation by GSK3ß inhibitors and mesoderm induction

(A) Luciferase assay of the ß-catenin promoter activity after treatment with increasing concentrations of GSK3ß inhibitors. A 6-point 3-fold serial dilution of each compound was performed (10, 3, 1, 0.3, 0.1, 0.03 μM, last 2 concentration data not shown). Columns show means +/− SD of 5 independent experiments. (B) Immunofluorescent localization of ß-catenin in hPSCs after a 24 hours treatment with either CP21 or CHIR. Representative image shown of 3 independent experiments on 3 different wells per condition. Scale bars: 50 μM (C) Quantitative PCR of ß-catenin target genes upon treatment of hPSCs with CP21 or

CHIR. Results shown are means and SEM of 3 independent experiments with 3 biological and technical replicates for each gene. (D) Immunofluorescence staining of hPSCs for markers of pluripotency, mesoderm and endoderm during the first 4 days of differentiation. Representative image shown of 3 independent experiments on 3 different wells per condition. Scale bars: 50 μM.

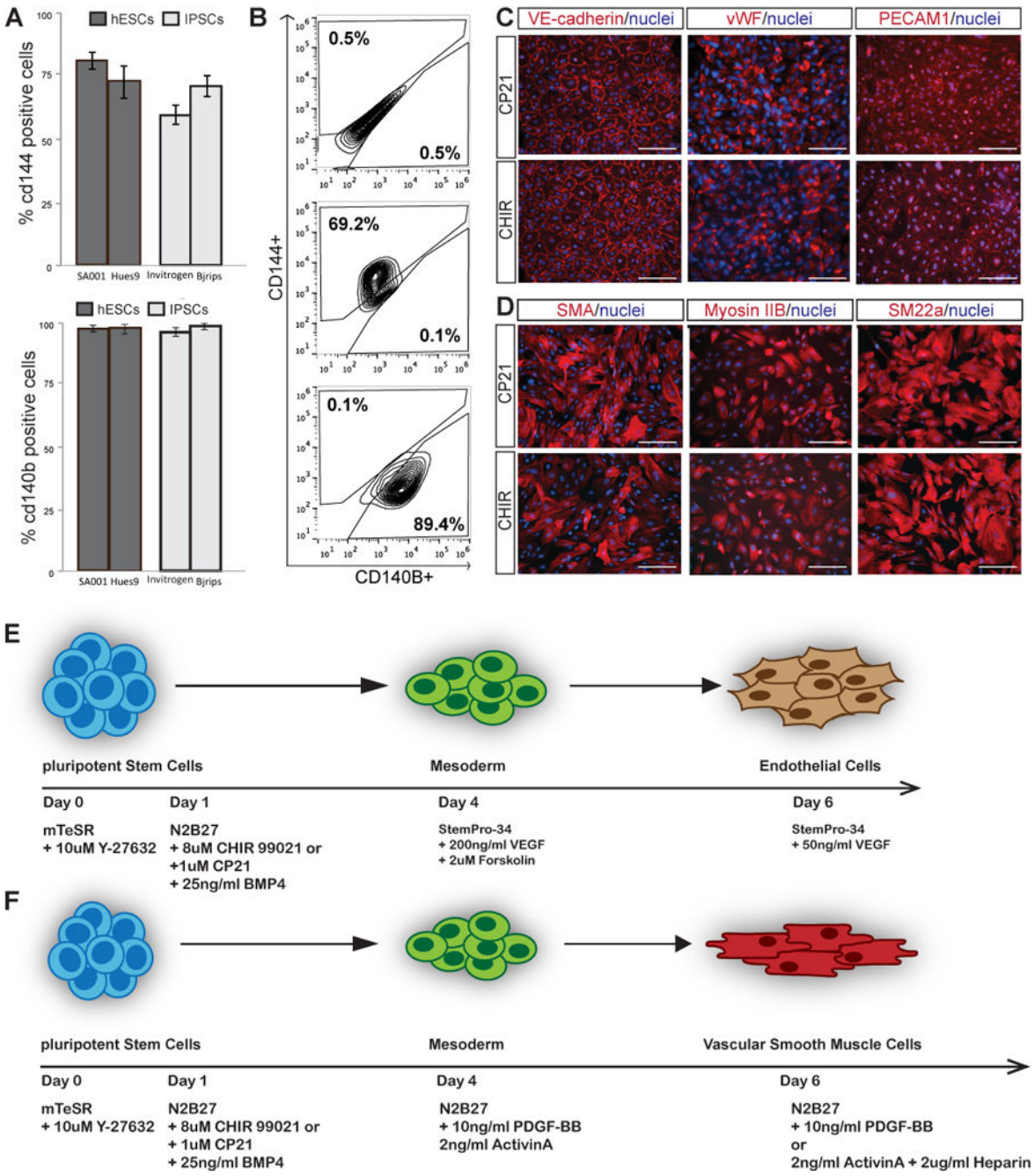

Figure 2. VEGF and PDGF-BB-mediated differentiation of hPSCs into vascular endothelial or vascular smooth muscle cells

(A) Differentiation efficiency of hPSC-ECs and hPSC-VSMCs from four different hESCs and iPSCs lines, (SEM 3.1, n=10 independent differentiation experiments) for hPSC-ECs and (SEM 2.7, n=16 independent differentiation experiments) for hPSC-VSMCs. Columns show means +/− SEM (B) Representative FACs plots from the differentiation experiments described in A): hPSCs (top panel) hPSC-derived ECs (middle panel) or hPSC-derived VSMCs (lower panel) stained for CD144 and CD140b. n= 10 (hPSC-ECs) and 16 (hPSC-VSMCs) independent differentiation experiments (C) Immunostaining of EC-specific

markers on hPSC-ECs; vWF=Von Willebrand factor. All cells (100%) were expressing VE-CAdherin and PECAM1 for both GSK3 inhibitors. 73.48% of the hPSC-ECs differentiated with CHIR and 74.52% of the cells differentiated with CP21 express vWF. Representative image shown of 3 independent experiments on 3 different wells per marker. Scale bars: 50 μM. (D) Immunostaining of VSMCs-specific markers on hPSC-VSMCs; SMA=smooth muscle actin alpha. For CHIR 48% of cells expressed SMA, 96.99% Myosin IIB and 98.7% SM22a. For CP21 62.08% of cells expressed SMA, 92.75% Myosin IIB and 100% SM22a. Representative image shown of 3 independent experiments. Scale bars: 50 μM. (E) Schematic illustration of EC differentiation strategy for hPSCs. (F) Schematic illustration of VSMCs differentiation strategy for hPSCs.

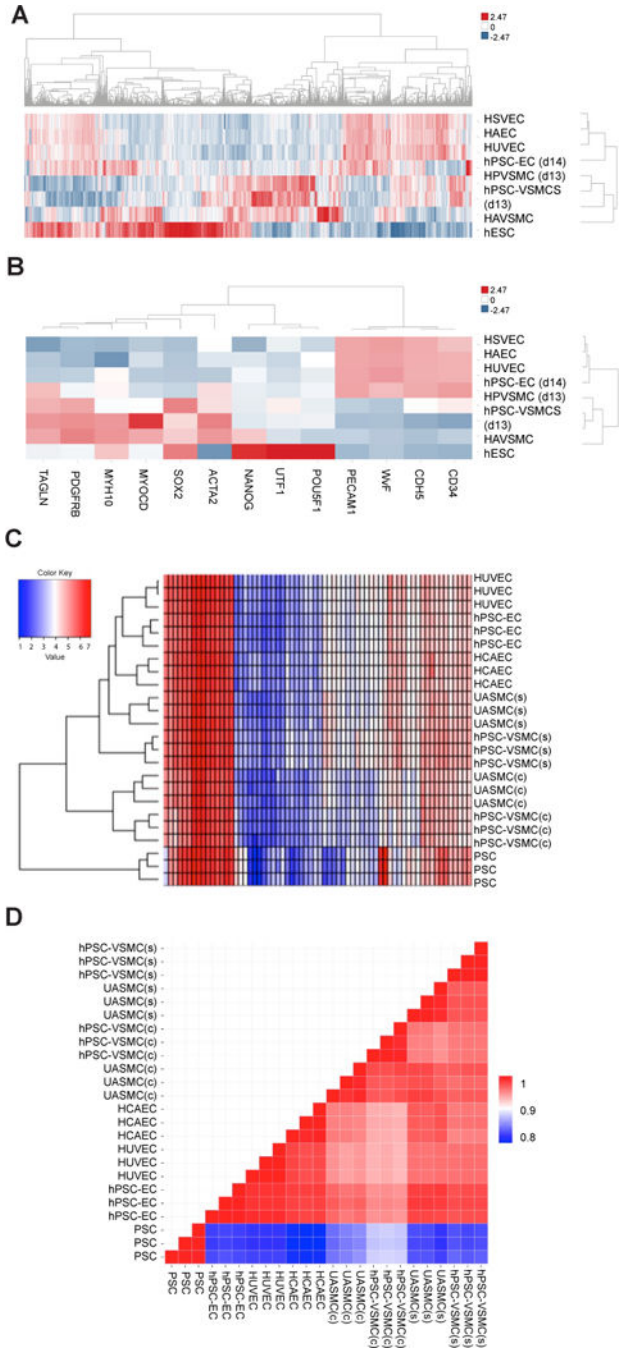

Figure 3. Global transcriptome and metabolomic analyses confirm vascular cell identity of differentiated hPSCs

(A) Global heat map of 2955 differentially expressed genes between embryonic stem cells (ESC) and differentiated endothelial cells (EC), vascular smooth muscle cells (VSMC), and primary cells (>10 fold change for at least one cell type). HUVEC= human umbilical vein EC, HSVEC= human saphenous vein EC, HAEC= human aortic EC, HPVSMC= human pulmonary VSMC, HAVSMC= human aortic VSMC. Columns represent genes, and rows are samples. Column Z-score transformation was performed on $\log_2$ expression values for each gene with blue denoting a lower and red a higher expression level according to the

average expression level. Hierarchical clustering of genes and samples is based on average linkage and correlation distance. (B) Heat map of marker genes panels for pluripotency, smooth muscle and endothelial cells across the same samples as in (A). Columns represent genes, and rows are samples. Column Z-score transformation was performed on $\log_2$ values for each gene with blue denoting a lower and red a higher expression level according to the average expression level. Hierarchical clustering of genes and samples is based on average linkage and correlation distance. (C) Heatmap of the metabolite composition of the different cell types clustered by similarities for the 66 metabolites detected intracellularly (see Supplemental Figure 5 for list of metabolites). Columns represent metabolites and rows represent samples. A dendogram beside the left y-axis illustrates clustering by similarity of metabolite value. There were n=3 cell line biological replicates for each cell type. Metabolite data was acquired as a single acquisition on mass spectrometer. Raw metabolite levels were $\log_2$ transformed to approximate a normal distribution. Red = higher values, blue = lower values. PSC= pluripotent stem cell, (c)= contractile and (s)= synthetic, UASMC= umbilical artery smooth muscle cell, HCAEC= human coronary artery EC. (D) Correlation matrix of spearman correlation coefficients of metabolite levels for each cell type. Color code represents strength of correlation: red = strongest correlation, blue = weakest. Spearman rank correlation performed on the non-parametric raw metabolite values and expressed as a correlation matrix (see Supplemental Figure 5 for list of metabolites). n=3 cell line biological replicates for each cell type. Metabolite data was acquired as a single acquisition on mass spectrometer. PSC = pluripotent parental stem cell, (c)= contractile and (s)= synthetic.

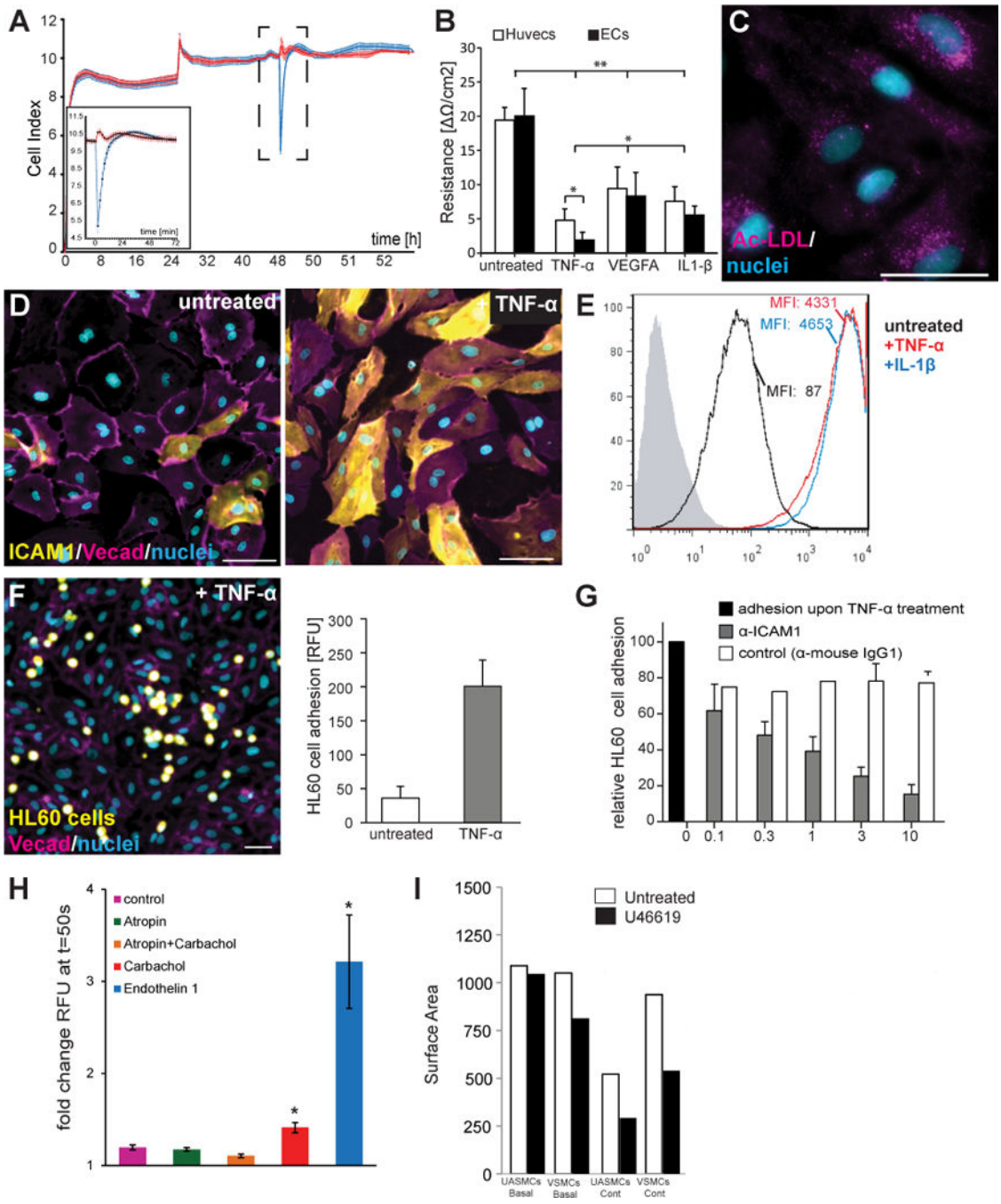

Figure 4. ***In vitro*** **characterization of hPSC-ECs and hPSC-VSMCs**

(A) Impedance-based monitoring of hPSC-EC monolayer culture. Thrombin treatment (blue, see inset) induced rapid decrease in impedance compared to control (red). One of the 4 independent experiments is depicted (n=8 technical replicates/experiment). Points represent mean +/− SD. (B) Trans-endothelial electrical resistance (TEER) properties of human umbilical cord endothelial cells (HUVECs) and hPSC-ECs either untreated or treated with 100ng/ml TNF-α; 100ng/ml VEGFA or 100ng/ml IL1; n=3 wells of 3 independent experiments (n= 9 wells in total except for untreated hPSC-ECs n=7 in total). Columns show

mean +/− SEM. Student *t*-test ** $p=5.56\times10^{-6}$; * $p=1.61\times10^{-5}$. (C) Uptake of fluorescently labeled acLDL by hPSC-ECs. Scale bars: 50μM. Representative image of 3 independent experiments. (D, E) Expression analyses of adhesion molecule ICAM1 upon treatment of hPSC-ECs with proinflammatory cytokines. Representative images and FACS plot from 3 independent experiments (3 technical replicates/experiment). (D) Immunofluorescence staining reveals upregulation of ICAM1 by TNFα treatment. Scale bars: 50μM. (E) Quantification of ICAM1 expression upon TNFα or IL1ß stimulation. (F) Immunostaining (left) and quantification of adhesion of leukocyte-like HL60 cells to hPSC-ECs upon TNFα stimulation. Scale bars: 50μM. Columns show mean +/− SD of 3 independent experiments. (G) Dose-dependent blockage of HL60 cell adhesion by anti-ICAM1 antibody pretreatment. Columns show mean +/− SD of 3 independent experiments (except for treatment with control antibody concentrations 0.1, 1. 3, here n=1) (H) Calcium imaging of SC-VSMCs at day 13 of differentiation. Stimulation with vasoconstrictive reagents resulted in increase in intracellular calcium. Fold change RFU to t=1 (before treatment) at t=50s (maximum peak). Columns show mean +/− SD of 3 independent assays and data were evaluated using Student's *t*-test; * = p=0.03 (I) Contractility assay on UASMCs and hPSC-VSMCs with U46619 48 hours after treatment. This graph shows one single experiment where control = 1 well and test = 2 wells per conditions.

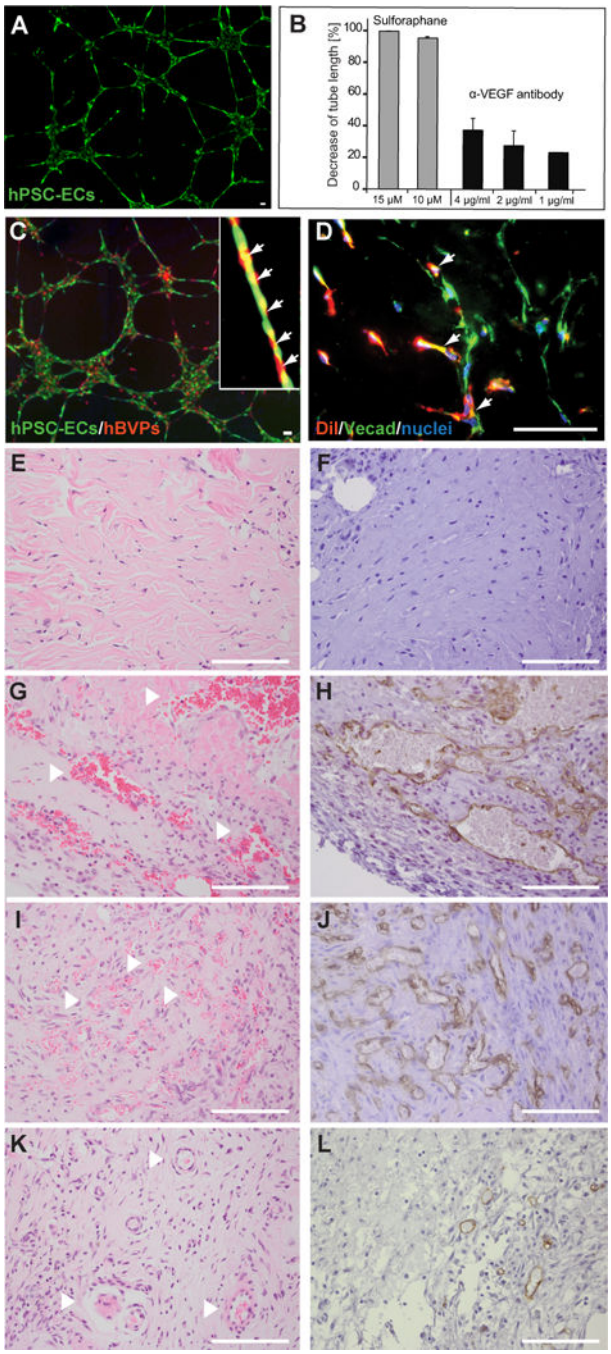

Figure 5. Co-culture experiments and *in vivo* characterization of hPSC-ECs

(A) *In vitro* tube formation assay of hPSC-ECs plated on matrigel for 24 hours, representative picture from 10 independent experiments. Scale bar: 50μm. (B) Quantification of the inhibitory effect of anti-angiogenic molecules on the tubologenesis of hPSC-ECs. Columns show means +/− SD of 3 independent experiments, (1ug/ml anti-VEGF, here n=1, no error bar) (C) Tube formation of hPSC-ECs with primary human brain vascular pericytes (hBVPs) (red) on matrigel after 24 hours. Scale bar: 50μm. (D) Close-up view in insert shows tubular structures formed by hPSC-ECs with closely associated hBVPs

(arrows), representative picture from 3 independent experiments. Scale bar: 50μm. (E-L) Representative pictures of fibrinogen grafts 14 days after implantation (except E and F, 7 days post implantation), (E,G,I,K) HE staining (F,H,J,L) human specific CD31/DAB staining. (E,F) hPSC-ECs only (G,H) HUVECs + MSCs (I,J) hPSC-ECs + MSCs and (K, L) hPSC-ECs+hPSC-VSMCs. This experiment was conducted once with 5 mice per conditions and 2 implants per mice (=10 implants per conditions). Scale bar: 50μm.